

# Direct Ethyl Levulinate Production from Raw Lignocellulosic Biomass Mediated by a Novel Taurine-Based Imidazolium Ionic Liquid

Gustavo R. Gomes,<sup>†</sup> Eupídio Scopel,<sup>‡</sup> Nicola L. Rocha, Márcia C. Breitkreitz, Rodrigo A. Cormanich, Camila A. Rezende,<sup>\*</sup> and Julio C. Pastre\*



Cite This: *ACS Sustainable Chem. Eng.* 2022, 10, 15876–15888



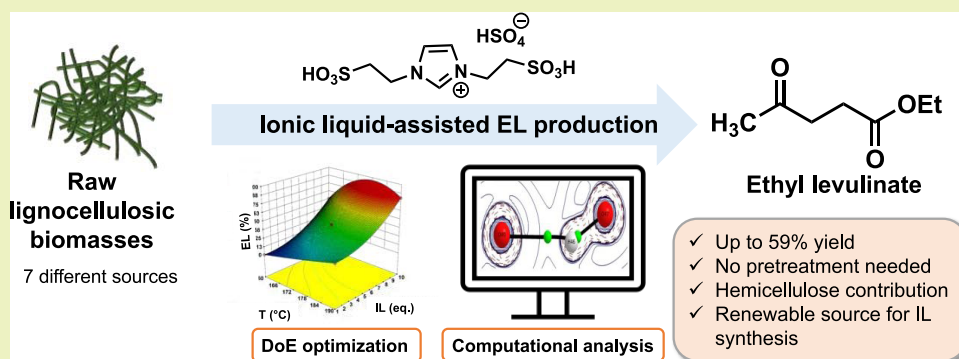
Read Online

ACCESS |

Metrics & More

Article Recommendations

Supporting Information



**ABSTRACT:** In this work, a novel renewable taurine-based ionic liquid (IL),  $[\text{TauIm}][\text{HSO}_4]$ , was synthesized *via* the Debus–Radziszewski reaction. The synthesized IL was then used to produce ethyl levulinate (EL) from several lignocellulosic substrates under microwave irradiation. Experimental conditions (temperature, time, and IL quantity) for EL production from a model substrate (microcrystalline cellulose, MCC) were first investigated by design of experiment (DoE) using a central composite design (CCD). The highest EL yields (over 80%) in MCC were achieved at the upper limits of all factors (190 °C; 60 min; 10 equiv of IL). Computational studies revealed that the IL–cellobiose interaction is stronger than the IL itself at the reaction temperature (190 °C), indicating the efficiency of the IL in interacting with cellulose in the optimal reaction conditions. Moreover, the formation of the IL–cellobiose complex was mediated by the hydrogen sulfate anion, while the cation worked as a spacer. Optimized conditions from DoE were also applied to sugarcane bagasse and straw, elephant grass leaves and stems, rice husks and straw, and corn biomass. EL production yields from 12 to 59% were obtained from these biomasses using this novel imidazolium IL, with the highest EL yields obtained with raw sugarcane bagasse (SCB) without any pretreatments. The superior performance of SCB was associated with the higher content of hemicelluloses in its composition compared to that of the other biomasses. Together, these results presented herein open new possibilities for increasing biomass valorization using renewable and straightforward routes.

**KEYWORDS:** ethyl levulinate, taurine, ionic liquid, lignocellulosic biomass, sugarcane bagasse

## INTRODUCTION

Lignocellulosic biomass is a renewable, abundant, and low-cost feedstock to replace the oil dependency for chemical, fuel, and material production.<sup>1</sup> Cellulose and hemicelluloses constitute up to 70 wt % of the lignocellulosic biomass composition and can be converted into various molecules of commercial interest by physical and chemical processes, for instance, ethyl levulinate (EL). EL is an important building block for plasticizers, green solvents, and pharmaceuticals.<sup>2</sup> Also, EL can be applied as a biofuel, with similar properties to biodiesel,<sup>3</sup> or as an additive to diesel (up to 5%) for improving fuel properties and reducing the emission of sulfur compounds into the atmosphere.<sup>4,5</sup> Likewise, EL can be used as a starting material to produce other high-value-added chemicals, such as 2-methyltetrahydrofuran (2-

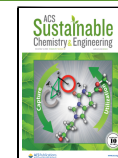
MeTHF),<sup>6</sup>  $\gamma$ -valerolactone,<sup>7</sup> valeric esters,<sup>8</sup> pyrrolidones,<sup>9</sup> 1,4-pentanediol,<sup>10</sup> among others.

However, carbohydrate conversion is commonly hindered due to the lignin present in the lignocellulosic biomass, which constitutes *ca.* 20–40 wt % of the raw substrate. Lignin can act as a physical barrier compromising the catalyst accessibility to the

Received: August 29, 2022

Revised: November 8, 2022

Published: November 21, 2022



sugar content.<sup>11</sup> Also, it can act as a chemical barrier interacting with the catalyst in the system, resulting in side reactions such as lignin depolymerization, especially the cleavage of aryl-ether linkages.<sup>12</sup> Therefore, the conversion of the biomass carbohydrates into valuable molecules is typically carried out in two steps: lignin extraction, commonly known as pretreatment, followed by carbohydrate conversion by chemical or biochemical processes.<sup>13</sup>

Ionic liquids (ILs) are suitable substances that can act as a solvent in biomass pretreatments (*i.e.*, fractionation of their compounds into cellulose, hemicellulose, and lignin) or in the further conversion of these fractions into final value-added compounds. ILs are salts with low melting points (usually below 100 °C), high thermal stability (up to 250 °C), low vapor pressure compared to conventional organic solvents, and adjustable polarity and miscibility, depending on the IL cation and anion compositions.<sup>14–16</sup>

As far as pretreatments are concerned, ILs mainly disrupt the strong chemical association between cellulose, hemicelluloses, and lignin in plant cell walls, leading to crystallinity decrease and delignification through carbohydrate solubilization.<sup>17,18</sup> In this scenario, the most studied ILs for biomass pretreatment are 1-alkyl-3-methylimidazolium derivatives, especially 1-butyl-3-methylimidazolium chloride [BMIM][Cl],<sup>19</sup> 1-butyl-3-methylimidazolium acetate [BMIM][OAc],<sup>20</sup> and 1-ethyl-3-methylimidazolium acetate [EMIM][OAc].<sup>21</sup> Recently, Uto and co-workers evaluated nine different ILs, concluding that 1-allyl-3-methylimidazolium chloride ([AMIM][Cl]) was the most effective for cellulose dissolution. In their work, the chloride anion had better performance than the acetate anion in the ILs, while the imidazolium cation with an allyl group provided a better interaction with cellulose, optimizing IL solubilization efficiency.<sup>22</sup> The effect of imidazolium IL in biomass deconstruction is associated with the presence of small and strong hydrogen bond acceptor anions, *e.g.*, chloride and acetate, which are able to permeate and disrupt hydrogen bonds between cellulose chains.<sup>23,24</sup> On the other hand, the imidazolium cation plays a secondary role in cellulose dissolution, acting as a spacer, *i.e.*, promoting the separation of cellulose chains.<sup>25</sup>

Regarding biomass conversion into high value-added chemicals, ILs can be applied to produce EL, replacing the typical acid-catalyzed approaches.<sup>26,27</sup> ILs can interact with the cellulose's intrinsic hydrogen bond network between strands resulting in a better solubilization/conversion than conventional acidic systems. Besides the aforementioned advantages of using ILs instead of mineral acids, ILs can reduce side reactions, lead to better selectivity, and avoid equipment damage caused by sulfuric acid, for example.

An ideal scenario to reduce costs and maximize the yields of EL is the direct production using raw feedstocks or waste materials to achieve value-added compounds by one-step procedures. However, direct biomass conversion usually results in lower yields due to the biomass intrinsic complexity. For this reason, there is still a reduced number of reports in the literature using acidic or IL-catalyzed processes to obtain EL from raw substrates, as can be exemplified in Table 1. Furthermore, most reports are still based on the acid-catalyzed conversion over long reaction times, mainly because of the use of conventional heating systems.

The reduced number of reports using ILs for the direct production of EL indicates that it is necessary to design efficient ILs that can convert the biomass carbohydrates in one step

**Table 1. Representative Examples for the Direct Production of EL from Raw Lignocellulosic Substrates Using Acidic or IL-Catalyzed Processes**

biomass	conditions <sup>a</sup>	EL yield	refs
bamboo	H <sub>2</sub> SO <sub>4</sub> 0.01 mol/L, 210 °C, 126 min	51 mol %	30
wheat straw	H <sub>2</sub> SO <sub>4</sub> 0.25 mol/L, 183 °C, 36 min	51 mol %	27
corn stover	H <sub>2</sub> SO <sub>4</sub> 0.1 mol/L, 160 °C, 30 min (microwave)	16 wt %	31
corn stover	H <sub>2</sub> SO <sub>4</sub> 0.29 mol/L, 190 °C, 30 min (microwave)	58 mol %	26
wheat straw	sulfonate IL (0.26 g/g biomass), 200 °C, 60 min	16 wt %	32
oil palm biomass	step 1: InCl <sub>3</sub> -IL(0.15 mmol/g), 177 °C, 4.8 h step 2: 105 °C, 12.2 h	20 wt %	33

<sup>a</sup>Ethanol used for EL production was of analytical grade.

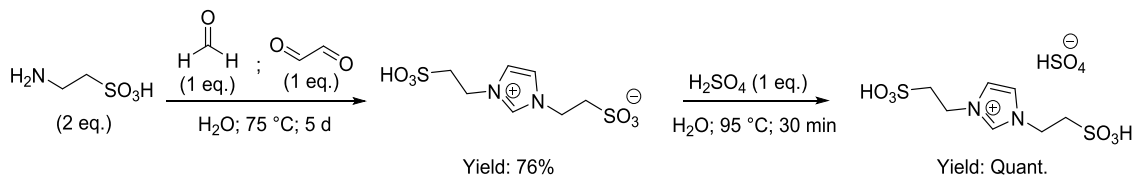
despite the recalcitrant biomass structure and possible interferents, such as lignin. Also, these ILs must be able to convert the lignocellulosic carbohydrates without the need for an exogenous catalyst (Lewis and/or Brønsted acids), which is commonly adopted in IL-assisted methodologies.<sup>28</sup> Therefore, a possibility is to design an IL that can act as a catalyst depending on the presence of appropriate functional groups in the IL structure, for instance, –COOH or –SO<sub>3</sub>H groups in the cation and/or anion.<sup>29</sup> Most notably, the presence of a sulfonic acid group plays a pivotal role in cellulose chemical conversion due to its high acidity compared to carboxylic groups. Moreover, these functional groups could lead to the synthesis of an IL that would play a bifunctional role, acting in pretreatment and conversion steps.

In addition to the compelling properties of using lignocellulosic biomasses as a source of valuable components, ILs must be synthesized using green strategies to result in a more sustainable process. Despite the outstanding contribution of imidazolium-based ILs for biomass processing, most are prepared using toxic chemicals derived from oil.<sup>34</sup> Therefore, using amino acids as starting material in a Debus–Radziszewski reaction stands out as a greener approach for synthesizing imidazolium ILs.<sup>35</sup> Bearing this in mind, Kirchhecker and co-workers described a methodology for synthesizing commercial imidazolium ILs using the Debus–Radziszewski reaction with amino acids, followed by a hydrothermal decarboxylation reaction.<sup>36</sup> A library of eight halogen-free ILs was generated using glycine, alanine, phenylalanine, and leucine with carbohydrate-related dicarbonyl compounds.

Taurine is an amino acid derivative from cysteine and methionine metabolism, and it is a natural compound that presents a sulfonic acid group in its structure.<sup>37</sup> Taurine is the main component of human bile and can be found in the heart tissue, brain, large intestine, and other parts of the human body.<sup>38</sup> This amino acid derivative is important in the food industry, in baby food, as nutritional supplements for athletes, and in energy drinks.<sup>39</sup> In our previous work, taurine hydrogen sulfate, [Tau][HSO<sub>4</sub>]<sup>–</sup>, a protic IL, was applied as a green Brønsted acid catalyst for the EL production from sugarcane molasses (sucrose-rich feedstocks) under microwave irradiation, affording EL in 82% from ash-free molasses.<sup>40</sup>

In this work, we synthesized a novel green taurine-based imidazolium IL, [TauIm][HSO<sub>4</sub>]<sup>–</sup>, which proved to be very efficient in converting biomass polysaccharides into EL under microwave irradiation. The yields achieved using the taurine-based IL were higher than the values reported using conven-

**Scheme 1.** Synthesis of [TauIm][HSO<sub>4</sub>]



tional acid-catalyzed processes. The performance of the synthesized IL was first evaluated in the conversion of MCC by a design of experiment (DoE) approach, and the best condition was then applied to various raw lignocellulosic biomasses, in which the presence of lignin did not hinder the carbohydrate conversion. The taurine-based imidazolium IL allowed the preparation of EL in high yields through a direct conversion without pretreatments. Computational analysis was performed to unveil the taurine-derived IL interactions with the cellulose structure and corroborated the DoE analysis and EL yields.

## EXPERIMENTAL SECTION

**Materials.** All chemicals used in this work were reagent grade. Taurine was obtained from Herbamix (Paulínia, São Paulo, Brazil); H<sub>2</sub>SO<sub>4</sub> was obtained from LS Chemicals (Mumbai, India); 40% w/v glyoxal in aqueous solution, EL standard, 1,3,5-trimethoxybenzene, and MCC were purchased from Sigma-Aldrich (St. Louis, Missouri); and 37% w/v formaldehyde in aqueous solution was obtained from Neon (Suzano, São Paulo, Brazil).

**Biomasses.** Sugarcane bagasse was donated by Raízen (Piracicaba, São Paulo, Brazil); sugarcane straw was donated by Ferrari Mill (Porto Ferreira, São Paulo, Brazil); elephant grass leaves and stems were donated by the Institute of Animal Science (Nova Odessa, São Paulo, Brazil); rice husks (variety IRGA 424) were purchased from a local rice mill (Porto Ferreira, São Paulo, Brazil); rice straw (variety EPAGRI 121 CL) was donated by the Comprehensive Technical Assistance Coordination (CATI, Guaratinguetá, São Paulo, Brazil); and corn biomass (variety DKB 340 PRO) was donated by local producers (Casa Branca, São Paulo, Brazil). All biomasses were dried in a convection oven (TECNAL TE 394/3) at 60 °C for 6 h and stored in plastic bags until use.

**Synthesis of the Taurine-Based IL, [Taulm][HSO<sub>4</sub>].** Taurine (20 mmol, 2.50 g), 10 mmol of 37% w/v formaldehyde in aqueous solution (745 μL), and 40% w/v glyoxal in aqueous solution (1.14 mL) were added in a round-bottom flask in 40 mL of distilled water (**Scheme 1**). The reaction was stirred for 5 days at 75 °C; after that, the water was removed in *vacuo* and the residue was washed with ethanol and filtered. The liquid fraction was also reduced under reduced pressure and further dried in *vacuum*, resulting in a pale yellow solid (76% yield; 2.15 g). For the acidification step, 1 equiv of the zwitterion was added to a round-bottom flask and acidified with 98% (533 μL) of H<sub>2</sub>SO<sub>4</sub> in 40 mL of distilled water at 95 °C for 30 min. After this period, the water was removed under reduced pressure, and the product was dried in *vacuum* for 48 h.<sup>41</sup> The [Taulm][HSO<sub>4</sub>] was obtained as a dark yellow liquid in quantitative yield. The NMR spectra of the compounds are presented in Figures S1 and S2 (Supporting Information).

[TauIm]: pale yellow solid; melting point: 123–127 °C;  $^1\text{H}$  NMR (250 MHz,  $\text{D}_2\text{O}$ ):  $\delta_{\text{H}}$  8.95 (s, 1H), 7.59 (d,  $J$  = 1.3 Hz, 2H), 4.63 (t,  $J$  = 6.5 Hz, 4H), 3.44 (t,  $J$  = 6.5 Hz, 4H);  $^{13}\text{C}$  NMR (62.5 MHz,  $\text{D}_2\text{O}$ ):  $\delta_{\text{C}}$  176.8; 122.6; 49.8; 45.2.

[TauIm]<sup>+</sup>[HSO<sub>4</sub><sup>-</sup>]: dark yellow liquid; <sup>1</sup>H NMR (250 MHz, D<sub>2</sub>O): δ<sub>H</sub> 8.90 (s, 1H), 7.54 (d, *J* = 1.6 Hz, 2H), 4.58 (t, *J* = 6.5 Hz, 4H), 3.40 (t, *J* = 6.5 Hz, 4H); <sup>13</sup>C NMR (62.5 MHz, D<sub>2</sub>O): δ<sub>C</sub> 136.7; 122.6; 49.8; 45.1; HRMS (ESI+): *m/z* calcd. for C<sub>7</sub>H<sub>13</sub>N<sub>2</sub>O<sub>6</sub>S<sub>2</sub><sup>+</sup> (cation): 285.02095; found: 285.02032.

**Procedure for the EL Production from Lignocellulosic Biomasses.** All experiments were carried out in a Biotage Initiator+ Microwave Synthesizer reactor using a 5 mL pressurized microwave

vial. In a typical experiment, 10 mg of the substrate (MCC or lignocellulosic biomass) and 3 mL of ethanol were applied for EL production. Temperature, time, and  $[\text{TauIm}][\text{HSO}_4]$  quantity varied according to the conditions defined by a central composite design (CCD), whose experimental matrix was a face-centered cube.

**Chromatographic Analyses.** EL was quantified by Gas Chromatography coupled to Mass Spectrometry (GC-MS) using an Agilent 7890 GC system, equipped with an Agilent HP-5MS column (60 m length, 0.25 mm diameter, 0.25  $\mu\text{m}$  film). The temperature ramp started at 60 °C for 1 min, then increased to 180 °C at a range of 20 °C  $\text{min}^{-1}$  and further increased to 280 °C at 30 °C  $\text{min}^{-1}$ , and then held for 2 min. The injector and MS source temperatures were 280 and 230 °C, respectively. The MS ionization impact was set at 70 eV, and the mass spectrometer was operated with a mass scan range of 30–400  $m/z$ . The EL quantification was carried out through internal calibration, using 1,3,5-trimethoxybenzene (TMB) as the internal standard. The response factor between EL and TMB and the EL concentrations were determined according to eq 1, where  $\text{Area}_{\text{EL}}$  and  $\text{Area}_{\text{IS}}$  are the areas from GC analysis of EL and internal standard, respectively. Furthermore,  $[\text{IS}]$  and  $[\text{EL}]$  are the concentrations of the internal standard and EL, respectively

$$\text{response factor} = \frac{\text{area}_{\text{EL}}}{\text{area}_{\text{IS}}} \times \frac{[\text{IS}]}{[\text{EL}]} \quad (1)$$

EL yields were determined by the theoretical yield (EL (%)) presented in eq 2, where  $m_{\text{experimental}}$  is the EL mass obtained experimentally determined by eq 1;  $m_0$  is the initial cellulose mass; 0.90 is the factor related to the cellulose acid hydrolysis to glucose equivalents; and 0.80 is the ratio between the molar masses of EL and glucose. When lignocellulosic materials are used for EL production, the hemicellulose contribution must be included, as presented in eq 3, where 0.88 is the factor related to the xylan acid hydrolysis and 0.96 is the ratio between the molar masses of EL and xylose, and the second  $m_C$  is thus related to the initial mass of hemicellulose

$$EL (\%) = \frac{m_{\text{experimental}}}{(m_0/0.90) \times 0.80} \times 100 \quad (2)$$

$$EL (\%) = \frac{m_{\text{experimental}}}{\{(m_0/0.90) \times 0.80\} + \{(m_0/0.88) \times 0.96\}} \times 100 \quad (3)$$

**Computational Details.** The computational procedure was based on the simulation of systems involving both anionic and cationic species of the studied IL and one molecule of cellobiose, the cellulose conformational unit. Initially, molecular dynamics (MD) calculations were performed for pairs of each ion on the IL (cation–cation and anion–anion interactions) and for the IL itself, using Desmond software.<sup>42</sup> The MD calculations could identify possible interactions between each pair of ions that may potentially decrease the population of cations and anions able to interact properly with molecules of cellobiose. Also, several MD calculations were carried out to understand the interactions between each pair of ions and cellobiose (anion–cellobiose and cation–cellobiose). Then, a last simulation was done with the three species (anion–cation–cellobiose). Simulations were based on molecular dynamics with 200 ns and Nosé–Hoover thermostat (NVT) at several temperatures (27, 127, 170, 175, 180, and 190 °C). *Ab initio* calculations at the M06-2X/6-31++(2d,p)<sup>43,44</sup> level were performed using the Gaussian 16 program<sup>45</sup> for complexes observed in the MD calculations at 190 °C. Geometry optimizations and single-point calculations were done at the same level. The IEFPCM

implicit solvent model<sup>46</sup> was used for single-point calculations, and counterpoise corrections were applied to the optimization step using the BSSE (basis set superposition error) model.<sup>47</sup> The results were compared with HF-LD (Hartree–Fock plus London dispersion) calculations run using ORCA software,<sup>48</sup> considered as a dispersion-corrected HF approach, where the dispersion interaction between two molecules is obtained at the DLPNO-CCSD(T) level.<sup>49</sup> Also, the energy of each interaction was estimated from QTAIM (quantum theory of atoms in molecules) calculations using the AIMALL software.<sup>50</sup>

**Biomass Chemical Composition.** Carbohydrates and lignin contents on the samples were determined following the NREL/TP-510-42618 method.<sup>51</sup> Sugar content was quantified by High Performance Liquid Cromatography (HPLC), acid-insoluble lignin was measured by gravimetry, and acid-soluble lignin was calculated by UV spectrometry at 280 nm. The extractives were determined according to the NREL/TP-510-42619 method.<sup>52</sup> The ash content was determined by gravimetry according to the NREL/TP-510-42622 method.<sup>53</sup>

**Sugarcane Bagasse (SCB) Pretreatments. Acid Treatment.** A diluted acid treatment using  $H_2SO_4$  1% v/v was carried out by treating 5 g of raw SCB (dry mass) in 50 mL of solution at 121 °C for 40 min in an autoclave. After the reaction time, the system was cooled down to room temperature, as previously described.<sup>54</sup> Then, the solid fraction was separated by filtration in a 149 µm mesh sieve and washed until neutral pH. Afterward, the biomass was dried in a convection oven at 60 °C for 6 h and stored.

**Acid–Base Treatment.** After acid treatment, the resulting solid was then treated with 3.5 wt % NaOH aqueous solution in a solid/liquid ratio of 1:25 (g/mL) at 120 °C for 90 min in an autoclave. Then, the system was cooled down to room temperature, filtered, dried, and stored, as described in acid treatment.

**Organosolv Treatment.** In the organosolv treatment, 5 g of raw SCB (dry mass) was mixed with 50 mL of 40% v/v ethanol (solid/liquid ratio 1:10) and heated up at 200 °C for 60 min. After that, the system was cooled down in an ice bath for 30 min. Then, the solid fraction was filtered and washed with 50 mL of ethanol and 100 mL of water, dried, and stored, as described in acid treatment.

**Statistical Analysis.** Statistical analysis of the regression models generated by DoE was carried out in the Design Expert Software (Stat-Ease, USA, version 13).

## RESULTS AND DISCUSSION

**Experimental Design for the IL-Assisted EL Production.** To evaluate the acidity strength of [TauIm][HSO<sub>4</sub>] in EL production from recalcitrant materials, a face-centered CCD was carried out using MCC as a model feedstock. The experimental matrix and the EL yields (%) are presented in Table 2. The factors evaluated were temperature ( $T$ : 160–190 °C), time ( $t$ : 20–60 min), and IL quantity (1–10 equiv), and their levels were selected according to previous works.<sup>40,55–57</sup> As can be seen in Table 2, the highest EL yield (81%) from MCC was achieved when all factors were at the upper level: 190 °C, 60 min, and 10 equiv of [TauIm][HSO<sub>4</sub>] (entry 8).

The statistic model that explains the EL yields from microcrystalline cellulose was a reduced cubic model (eq 4), in which  $A$  is related to the temperature,  $B$  to the time, and  $C$  to the IL loading. The linear coefficients presented the highest values for the coefficients. The quantity of [TauIm][HSO<sub>4</sub>] ( $C$ ) used in the synthesis proved to be the most important contribution for the model, with a positive contribution of +36.00, followed by time ( $B$  = +19.00) and temperature ( $A$  = +17.30), both with a positive contribution

**Table 2. Face-Centered CCD for EL Production from MCC Mediated by [TauIm][HSO<sub>4</sub>]<sup>a</sup>**

entry	$T$ (°C)	$t$ (min)	IL (equiv)	EL (%)
1	160	20	1	nd
2	190	20	1	15
3	160	60	1	1
4	190	60	1	30
5	160	20	10	12
6	190	20	10	75
7	160	60	10	51
8	190	60	10	81
9	160	40	5.5	4
10	190	40	5.5	40
11	175	20	5.5	6.3
12	175	60	5.5	44
13	175	40	1	1
14	175	40	10	73
15	175	40	5.5	17
16	175	40	5.5	22
17	175	40	5.5	24
18	175	40	5.5	24
19	175	40	5.5	18

<sup>a</sup>nd, not detected.

$$\begin{aligned} \text{EL} (\%) = & -11.88 A^2 B - 14.38 A^2 C - 5.88 ABC - 2.04 \\ & A^2 + 12.96 C^2 - 2.37 AB + 6.13 AC + 3.63 \\ & BC + 17.30 A + 19.00 B + 36.00 C \end{aligned} \quad (4)$$

In terms of second-order effects, the square of the IL amount was more significant ( $C^2$  = +12.96), while the other quadratic effects provided low coefficient values. Cubic interactions had great significance on the model, and their highest value was the interaction between square temperature and IL ( $A^2C$  = −14.38). The relevant contribution of cubic effects showed that EL production from cellulose is a complex system. The ANOVA (Table S1) showed that the regression was significant ( $p < 0.0001$ ), without lack of fit ( $p > 0.4581$ ), meaning that the experimental factors impact the response and that the proposed reduced cubic model is valid. Also, the experimental values agree with the values predicted by the reduced cubic model (Figure S3). The coefficients of determination ( $R^2$ ), adjusted  $R^2$ , and predicted  $R^2$  were 0.9934, 0.9830, and 0.8967, respectively, indicating the adequacy of the model and accuracy of predictions of the EL yield from microcrystalline cellulose.

When the time is fixed at its lower level (20 min), the region of high EL yields converges to the upper levels of temperature and IL quantity, 190 °C and 10 equiv, respectively (Figure 1A). On the other hand, when the time is fixed at its upper level (60 min), the response surface shows a curvature effect. At high IL amounts, there is a local apex in the temperature axis near 185 °C (Figure 1B).

Therefore, the CCD design for the EL production from MCC indicated that higher EL yields (over 80%) could be achieved at the upper levels of all evaluated factors, temperature, time, and IL quantity. The best results were obtained at the typical temperatures reported in the literature (Table 1), however, in a reduced time compared to the conventional heating systems, which indicates the efficiency of using microwave irradiation in this work.

**Understanding the Molecular Interactions by Computational Studies.** As [TauIm][HSO<sub>4</sub>] is a new IL, we wish to

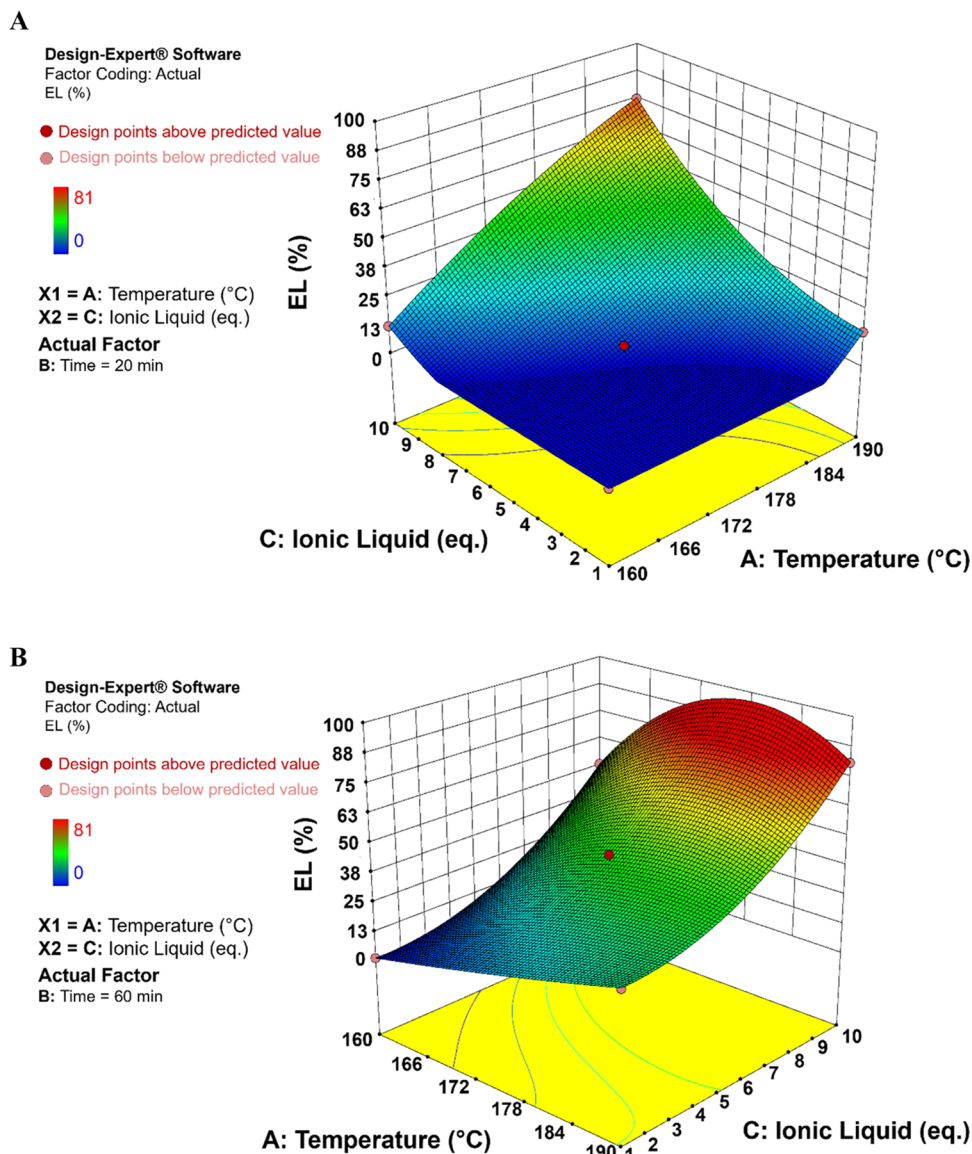


**Figure 1.** Response surfaces for EL production from microcrystalline cellulose as a function of temperature and IL (equiv) when time is fixed at (A) 20 min and (B) 60 min.

further investigate how the taurine-based IL interacts with the cellulose to explain biomass deconstruction and the conversion to EL. Thus, molecular dynamics (MD) and *ab initio* calculations were carried out to shed light on the main interactions between the IL and cellulose. Cellobiose, the cellulose conformational unit,<sup>58</sup> was used as the sugar model for these calculations. Six different systems were investigated, three involving the IL itself: cation–cation, anion–anion, and cation–anion; and three systems involving the ionic species and cellobiose: cation–cellobiose, anion–cellobiose, and cation–anion–cellobiose. MD calculations for these systems were carried out at several temperatures to estimate in which of them the interactions between these ion pairs could be identified (Figure S7). The obtained complexes in the MD calculations at 190 °C were used as input for the *ab initio* calculations, from which the complexation energy and dissociation energy were obtained. Complexation energies were also calculated using the HF-LD method<sup>49</sup> as the benchmark. Compared to *ab initio* calculations performed at the M06-2X/6-31++(2d,p) level of

theory, the results showed an absolute mean error of only 1.79 kcal mol<sup>-1</sup> when five complexes were used (Table S2).

Some hydrogen bond interactions could be observed for the cation–cation model (Figure S4). The graphs in Figure S7F,G indicate the number of occurrences of hydrogen bond interactions in the cation–cation model, which showed a low occurrence during the calculated simulation time (only one or two interactions in approximately 10 ns of simulation). Due to the absence of interactions at 190 °C, the individual interactions and complexation energies were not calculated by *ab initio* methods. On the other hand, complexes between hydrogen sulfate anions (Figure S5) were found at temperatures up to 185 °C (Figure S7A–E). The main complex found in the MD simulations was used as input for *ab initio* calculations, giving a stabilizing complexation energy of -8.93 kcal mol<sup>-1</sup>, presumably related to hydrogen bonds involving the hydroxyl groups O10H6 and O2H7 (Figure S5). However, a negative value of  $\Delta G_{\text{diss}}$  (-1.78 kcal mol<sup>-1</sup>) at 25 °C was also observed, indicating that the complex dissociation should be spontaneous at this temperature.

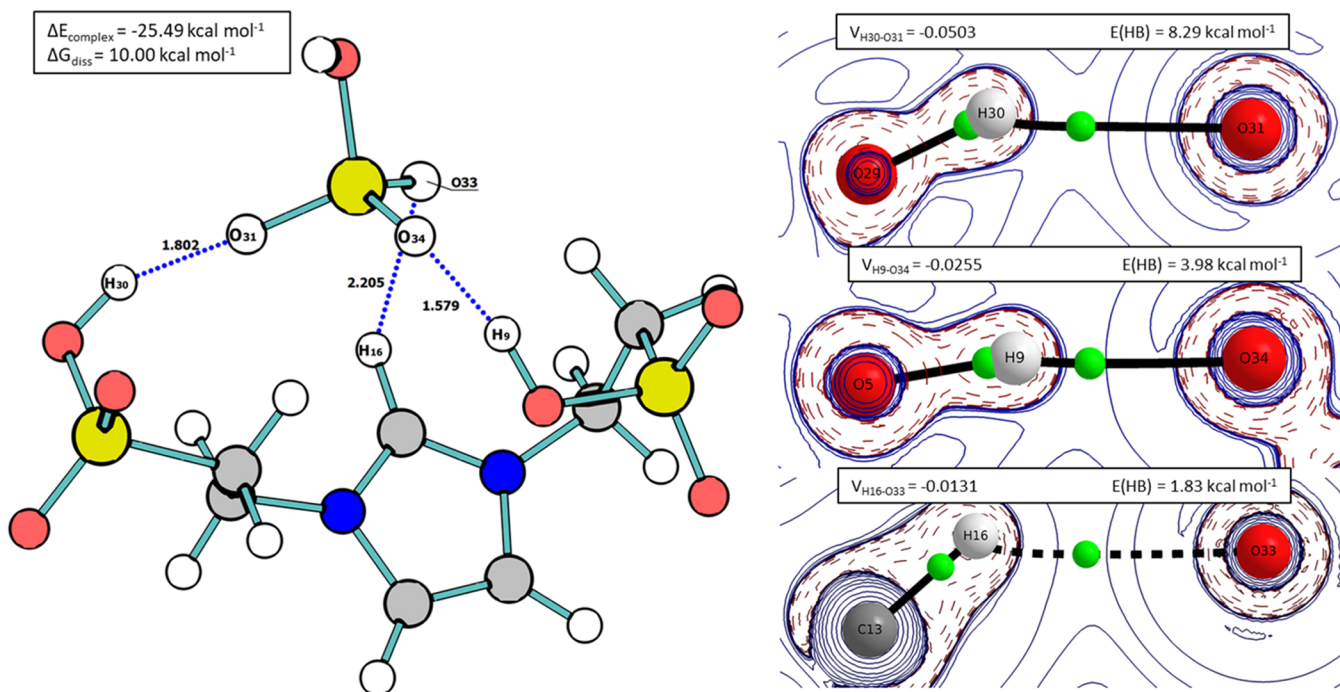


**Figure 2.** Intermolecular complex between taurine-derived imidazolium cation and hydrogen sulfate anion ( $[\text{TauIm}][\text{HSO}_4]$ ) observed at  $190^\circ\text{C}$ . Interaction energies were calculated using QTAIM calculations by applying the equation  $E_{\text{HB}}(V) = 0.277|V|-0.45$ . Thermodynamic properties were obtained by DFT calculations (M06-2X/6-31++(2d,p)). Dashed lines represent the observed hydrogen bond interactions (hydrogen bond distance values given in angstroms).<sup>59,60</sup>

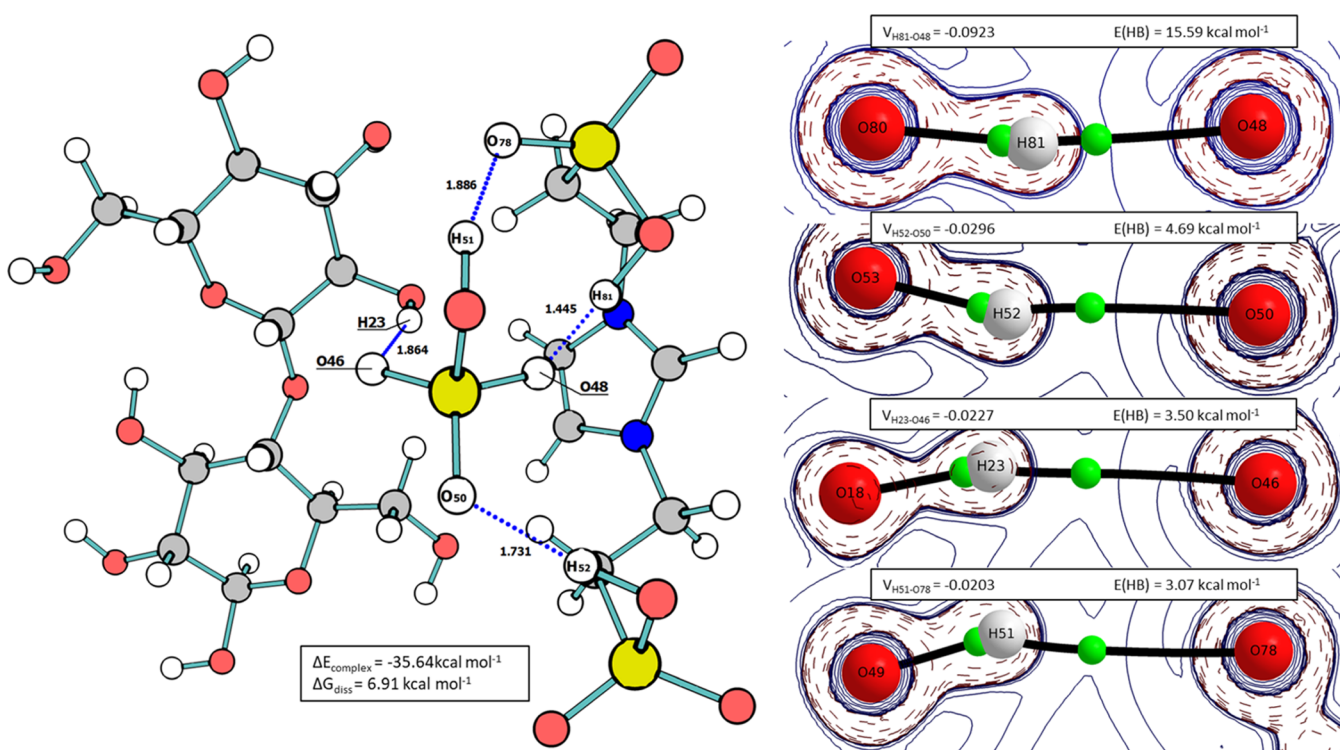


**Figure 3.** Intermolecular complex between  $[\text{TauIm}][\text{HSO}_4]$  and cellobiose observed at  $190^\circ\text{C}$ . Interaction energies were calculated using QTAIM calculations by applying the equation  $E_{\text{HB}}(V) = 0.277|V|-0.45$ . Thermodynamic properties were obtained by DFT calculations (M06-2X/6-31++(2d,p)). Dashed lines represent the observed hydrogen bond interactions (hydrogen bond distance values given in angstroms).<sup>59,60</sup>

The interactions between the taurine-derived imidazolium cation and hydrogen sulfate anion (Figure 2) could be observed in all calculated temperatures (Figure S7J). The taurine-derived imidazolium cation complex showed a high energetic stabiliza-

tion ( $\Delta E_{\text{complexation}} = -25.49 \text{ kcal mol}^{-1}$ ) and a positive  $\Delta G_{\text{diss}}$ , indicating that the dissociation is not a spontaneous process at  $25^\circ\text{C}$ .

Intermolecular interactions between  $[\text{TauIm}][\text{HSO}_4]$  and cellobiose (Figure 3) also occur at high temperatures (higher than 180 °C). As aforementioned, MD calculations indicated that hydrogen sulfate anions have a low tendency to form dimers at temperatures up to 190 °C and should be available to form  $[\text{TauIm}][\text{HSO}_4]$  and complexes with cellobiose.

*Ab initio* calculations revealed a high stabilization in the  $[\text{TauIm}][\text{HSO}_4]$ /cellobiose complex, with  $\Delta E_{\text{complex}} = -35.64 \text{ kcal mol}^{-1}$ , higher than the stabilization energy of the IL itself ( $\Delta E_{\text{complex}} = -25.49 \text{ kcal mol}^{-1}$ ) and about four times higher than the stabilization between hydrogen sulfate anions ( $\Delta E_{\text{complex}} = -8.93 \text{ kcal mol}^{-1}$ ). The complex stability increase may be related to the high number of hydrogen bonds, whose energies range from 3.07 to 15.59 kcal mol<sup>-1</sup>, as shown in Figure 3. Also, the  $[\text{TauIm}][\text{HSO}_4]$ /cellobiose complex has a positive  $\Delta G_{\text{diss}}$ , meaning a nonspontaneous dissociation at 25 °C.

The mean geometry obtained by MD calculations showed that the  $[\text{TauIm}][\text{HSO}_4]$ /cellobiose complex formation occurs by the mediation of the hydrogen sulfate anion. This observation is aligned with the literature since the anion disrupts the cellulose inter- and intramolecular hydrogen bond networks, and the cation works as a spacer, separating the cellulose chains and providing solubilization.<sup>22,25</sup> This tendency of hydrogen sulfate anion to act as a mediator can be rationalized by analyzing the complex  $[\text{TauIm}][\text{HSO}_4]$  (Figure 2). Three interactions could be identified in this model with energies between 1.8 and 8.3 kcal mol<sup>-1</sup>. On the other hand, the complex formed between the three species (anion–cation–cellobiose; Figure 3) showed four interactions with energies between 3.0 and 15.5 kcal mol<sup>-1</sup>. In this case, the weakest interaction previously shown by the  $[\text{TauIm}][\text{HSO}_4]$  complex ( $E_{\text{H16-O33}} = 1.8 \text{ kcal mol}^{-1}$ ) was replaced by a new interaction between cellobiose and the hydrogen sulfate anion ( $E_{\text{O46-H23}} = 3.5 \text{ kcal mol}^{-1}$ ), increasing the complex stability. The interaction preference between the taurine cation and the hydrogen sulfate anion, however, could be rationalized by the energies shown in the complex  $[\text{TauIm}][\text{HSO}_4]$ , greater than the energies shown by the complex formed between the cellobiose molecule and the taurine-derived imidazolium cation (between 1.4 and 7.0 kcal mol<sup>-1</sup>; Figure S6B,C).

Therefore, the computational analysis provided important explanations for the observed experimental results. The  $[\text{TauIm}][\text{HSO}_4]$ /cellobiose complex is more stable than the IL itself, and the loss of hydrogen sulfate anion self-interaction at 190 °C can explain the efficient cellulose conversion to EL mediated by  $[\text{TauIm}][\text{HSO}_4]$  at this temperature. In addition, computational analysis concords with the statistical tendency described in the previous section, which indicated that higher EL yields from microcrystalline cellulose are obtained above 180 °C.

**EL Production from Lignocellulosic Biomasses Mediated by  $[\text{TauIm}][\text{HSO}_4]$ .** As the  $[\text{TauIm}][\text{HSO}_4]$  proved to efficiently convert a cellulosic model (MCC) to EL at high yields, sugarcane bagasse (SCB) was then tested as a lignocellulosic feedstock for EL production mediated by the taurine-derived imidazolium IL. Lignocellulosic substrates are more complex than MCC in terms of chemical composition and structure but are more feasible for EL production at an industrial scale because they are readily available. SCB was selected to be evaluated first due to its large-scale production as an agroindustrial residue in countries like Brazil, where the annual sugarcane production is estimated at more than 592.031 tons in 2021/22.<sup>61</sup>

Experiments using raw SCB were carried out at the best conditions determined for EL production from MCC (190 °C, 60 min, and 10 (equiv) IL), resulting in a 59% EL yield (Table 3). This is an excellent result compared to the reported values in

**Table 3. Pretreatment Evaluation for the EL Synthesis from SCB<sup>a</sup>**

chemical composition (%)	pretreated SCB			
	raw SCB	acid <sup>b</sup>	organosolv <sup>c</sup>	acid–base <sup>d</sup>
cellulose	38.9 ± 1.5	59.0 ± 1.0	71.6 ± 1.6	82.0 ± 0.2
hemicelluloses	28.9 ± 1.1	7.6 ± 0.6	11.2 ± 0.1	7.1 ± 0.8
lignin	32.0 ± 1.0	31.7 ± 0.6	14.8 ± 0.2	13.1 ± 0.6
ashes	2.5 ± 0.6	3.0 ± 1.0	1.5 ± 0.1	5.0 ± 1.0
extractives	2.1 ± 0.2	nd	nd	nd
pretreatment yield		68 ± 1	42 ± 3	32 ± 1
EL	59 ± 4	44 ± 5	52 ± 5	55 ± 6

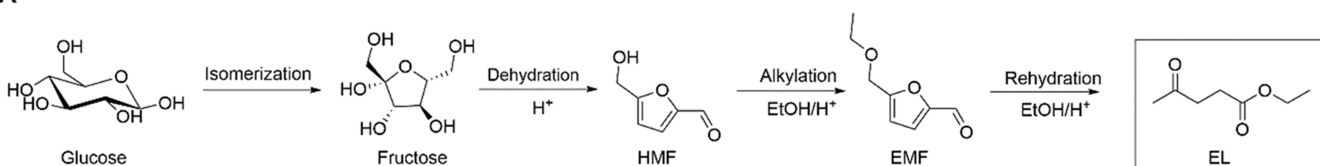
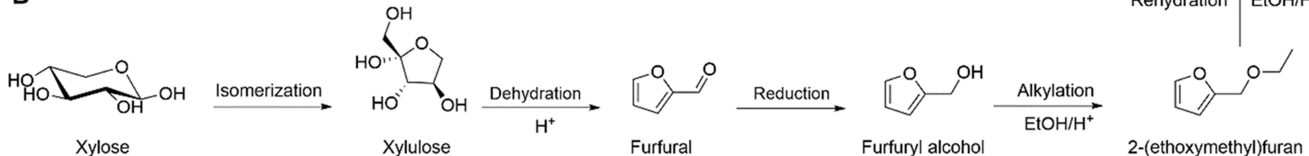
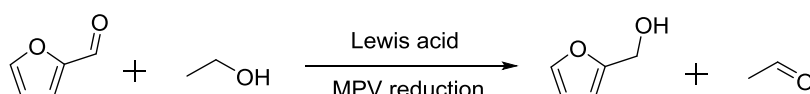
<sup>a</sup>Conditions: SCB: 10 mg;  $[\text{TauIm}][\text{HSO}_4]$ : 10 equiv; EtOH: 3 mL; T: 190 °C; t: 60 min; MW, experiments in triplicate. <sup>b</sup>T: 121 °C; t: 40 min;  $\text{H}_2\text{SO}_4$  1% v/v; solid/liquid 1:10. <sup>c</sup>Solvent: EtOH 40%; T: 200 °C; t: 60 min; solid/liquid 1:10. <sup>d</sup>Acid: T: 121 °C; t: 40 min;  $\text{H}_2\text{SO}_4$  1% v/v; solid/liquid 1:10.; base: T: 120 °C; t: 90 min; NaOH 3.5%; solid/liquid 1:25. nd: not detected.

the literature, even compared to those that use mineral acid-catalyzed systems (Table 1). This EL yield points out the efficiency of  $[\text{TauIm}][\text{HSO}_4]$  in converting raw feedstocks into value-added chemicals such as EL, despite their high lignin content (32%).

EL production was also evaluated using SCB substrates obtained after conventional pretreatment strategies: acid, acid–base, and organosolv pretreatments (Table 3). Surprisingly, the EL yields did not increase using the cellulose-enriched pretreated solids. The EL yield from the acid-treated SCB was considerably lower (44%) compared to that of the raw SCB (59%), despite its higher cellulose content (39% in the raw SCB and 59% in the acid-treated SCB). This yield reduction is probably a consequence of the significant removal of hemicelluloses (reduction of 86%) due to the acid treatment. Another sign that supports the hemicellulose positive influence in the higher EL yield is that the lignin content in the acid-treated solid is the same as in the raw substrate, indicating that the difference in the chemical yield is not related to the lignin content.

Several factors are known to affect the susceptibility of glycosidic linkages to acid hydrolysis, including inductive and steric effects, the hemiacetal ring conformation, the degree of macromolecular interactions, and the presence of decorations in the main backbone. Glycosidic linkages between sugars containing a furanosidic ring, such as in the case of the  $\alpha$ -(1–3) linkage between xylose and arabinose, have lower resistance to acid hydrolysis compared to a pyranosidic one. This difference is related to the conformational stability of the carbohydrate hemiacetal ring. A six-membered ring is more stable because the ring does not present any tension in the structure; on the other hand, a five-membered ring has a slightly angular tension, which gives some instability to the molecule.<sup>62</sup>

After the hydrolysis of polysaccharides (cellulose and hemicelluloses) to monomeric sugars, the EL production from pentoses follows a different pathway compared to hexoses, as represented in Scheme 2. The hexose pathway starts with the isomerization step, then conversion of a six-membered to a five-membered ring (fructose), followed by dehydration to HMF,

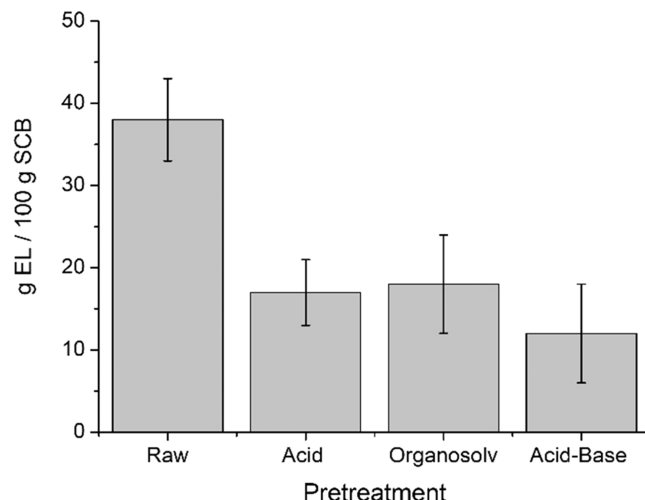
**Scheme 2. Chemical Pathways for EL Production from (A) Hexoses and (B) Pentoses****A****B****Scheme 3. Furfuryl Alcohol Formation via MPV Reduction**

alkylation to EMF, and finally rehydration to EL.<sup>40,63</sup> The pentose pathway follows xylose isomerization to xylulose and dehydration to furfural, similarly to glucose. On the other hand, there is an additional step, which is the furfural reduction to furfuryl alcohol; then, alkylation and rehydration steps take place.<sup>63</sup>

The results described in Table 3 show a contribution of the hemicellulose fraction on EL production from SCB. However, to achieve EL as a final product, it is necessary to go through a reduction step, as described in Scheme 2. One proposal to explain EL formation from hemicelluloses considers that furfuryl alcohol is produced via the Meerwein–Ponndorf–Verley (MPV) reduction reaction (Scheme 3).<sup>64,65</sup> Since ethanol is the solvent, it could act as a H-donor for furfural reduction. Also, for this reaction to occur, the presence of a Lewis acid is necessary, usually a metal catalyst. The ash fraction in SCB contains strong Lewis acids in its composition, such as Si (92.8 wt %) and Al (3.0 wt %),<sup>66</sup> which could act as a catalyst for furfural MPV reduction to produce furfuryl alcohol *in situ*.

By evaluating the other pretreatments, the sequential lignin extraction using an alkali treatment in the acid-treated substrate resulted in a cellulose-rich solid (82%) with a similar content of hemicellulose than the acid substrate (7%) but with a reduced quantity of lignin (13%). Nevertheless, EL yields obtained from this substrate were statistically the same as the raw SCB, indicating again that the presence of lignin in the raw substrate was not a significant interferent for EL production. Similarly, organosolv pretreatment reduced 54% of the raw lignin content and did not significantly influence EL yields, which was statistically similar to the raw SCB. Indeed, organosolv pretreatment also showed an important loss in hemicelluloses (reduction of 61%) through lignin–carbohydrate extraction, negatively affecting the EL yields.

Considering the pretreatment yields and the EL yields, the raw SCB was the best substrate for the chemical conversion, providing 38 g of EL per 100 g of SCB (Figure 4). The mass yields (mass of EL (g) per 100 g of processed biomass) from pretreated materials were considerably low compared to the raw SCB due to weight losses during the pretreatment. Acid and organosolv pretreatments provided similar results, around 17 g

**Figure 4. Mass EL yields (g EL/ 100 g SCB) from raw and pretreated SCBs.**

EL/100 g SCB, while acid–base pretreatment provided the lowest yield, 12 g EL/100 g SCB, due to high mass losses during the two-step pretreatment. Together, these results indicate that there is no necessity to perform a pretreatment step to achieve high EL yields from SCB. Therefore, the strong chemical association between the macromolecular components did not affect the solubilization/conversion ability of the taurine-derived IL, [TauIm][HSO<sub>4</sub>].

As raw SCB showed the best results, we also evaluated the taurine-based IL performance in other raw lignocellulosic materials, such as sugarcane straw (SCS), elephant grass leaves (EGL), elephant grass stem (EGS), rice straw (RS), rice husk (RH), and corn biomass (CB). The chemical composition of all biomasses is presented in Table S3. According to Figure 5, SCB is still the most promising lignocellulosic biomass for EL production, while the other biomasses presented EL yields varying from 26 to 43%. As evaluated in the pretreated SCB substrates, the higher content of hemicelluloses is probably the factor that contributes the most to the SCB high yields observed for SCB, in comparison to the other biomasses. Indeed, this

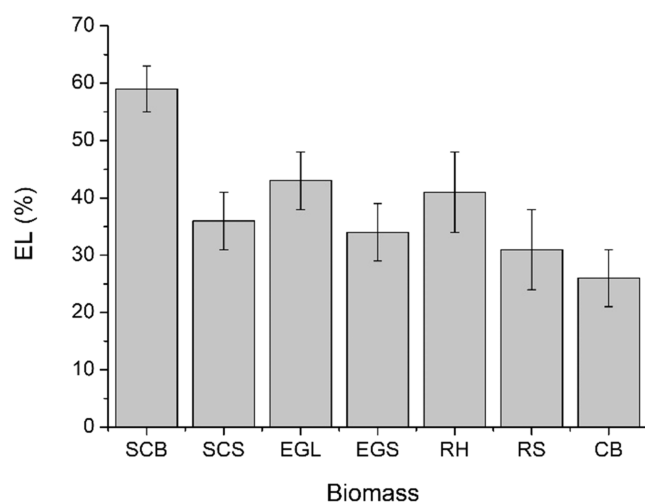


Figure 5. EL production from different lignocellulosic materials.

contribution is observed due to the linear correlation between the hemicellulose content and the EL yields in different raw biomass (Figure S8), which means that the higher the content of hemicelluloses in the composition, the higher the EL yields. Making a comparison between feedstocks from the same plant, it can be noticed that a higher ash content resulted in a higher EL yield: SCB (ash: 2.5%; EL: 59%) and SCS (ash: 1.5%; EL: 36%); EGL (ash: 5.7%; EL: 43%) and EGS (ash: 3.2%; EL: 34%); RH (ash: 14.8%; EL: 41%) and RS (ash: 3.6%; EL: 31%). As described above, this observation can be related to furfural reduction via MPV reaction.

**Evaluating the Green Credentials for EL Production Mediated by [TauIm][HSO<sub>4</sub>].** Proving that the renewable taurine-derived IL, [TauIm][HSO<sub>4</sub>], had an excellent performance for EL production from real feedstocks, we first turned our attention to the evaluation of the green credentials of [TauIm][HSO<sub>4</sub>]. To do so, we selected two important green metrics, the process mass intensity (PMI) and the renewable percentage (RP), to evaluate the greenness of the [TauIm]-

[HSO<sub>4</sub>] synthesis. Since the solvent typically contributes significantly to synthetic procedures at the laboratory scale, we selected the PMI from reagents, reactants, and catalysts (PMI<sub>RRC</sub>) to make a fair comparison with the literature. The PMI<sub>RRC</sub> is the ratio between the total mass of reagents, reactants, and catalysts by the mass of the product, as described in eq 5<sup>67</sup>

$$\text{PMI}_{\text{RRC}} = [m_{\text{reagents}} + m_{\text{reactants}} + m_{\text{catalyst}}]/m_{\text{product}} \quad (5)$$

The second metric selected is the renewable percentage (RP), composed of two main terms. The first one is the renewable intensity (RI), which is the ratio of the mass of all renewables used in the synthesis to the mass of the product (6). Then, the renewable percentage is the relation between RI and PMI, as described in eq 7<sup>68</sup>

$$\text{RI} = \text{mass of all renewables used}/\text{mass of product} \quad (6)$$

$$\text{RP} (\%) = \frac{\text{RI}}{\text{PMI}} \times 100 \quad (7)$$

Then, we selected some sulfonated-based IL described in the literature to compare the [TauIm][HSO<sub>4</sub>] synthesis (Table 4, entry 7) with other examples previously reported (Table 4, entries 1–6). As described in Table 4, most ILs evaluated present an excellent PMI value for the synthesis (closer to 1), indicating that the mass used for the starting materials (reactants, reagents, and catalysts) is incorporated into the product. However, some of these processes used petrochemical-based reactants such as 1,4-butanesulfone and 3-methylpyridine, resulting in a null renewable percentage.

A closer inspection of Table 4 reveals the examples that resulted in good RP that used amino acid derivatives in their synthesis (for example, proline, choline, and taurine). The cholinium IL reported by Lee and co-workers presented an RP below 50% (46%) due to the negative contribution of chlorosulfonic acid in the synthesis. On the other hand, the protic ILs from direct acidification of amino acid derivatives presented RP between 50 and 60%, which could be explained by the contribution of sulfuric acid used in their preparation. As direct acidification is an equimolar reaction, nearly half the total

Table 4. Green Metrics for the Synthesis of Several Sulfonated-Based IL Described in the Literature <sup>a,b</sup>

Entry	IL	PMI <sub>RRC</sub>	RP (%)	Ref.
1		4.1	-	71
2		1.1	-	32
3		1.1	-	72
4		1.1	46	73
5		1.1	52	74
6		1.0	59	40
7		1.4	77	This work

<sup>a</sup>PMI<sub>RRC</sub>: process mass intensity of reagents, reactants, and catalyst. <sup>b</sup>RP: renewable percentage.

mass came from sulfuric acid. Consequently, the renewable intensity drops by half affecting the final percentage. The [TauIm][HSO<sub>4</sub>] has the higher RP (77%) among the described examples since all reagents used to make the imidazole ring through the Debus–Radziszewski reaction, taurine, formaldehyde,<sup>69</sup> and glyoxal<sup>70</sup> can be obtained from renewable sources.

We also evaluate the metrics for EL production from raw and pretreated SCBs to quantitatively show that pretreatment steps are unnecessary when [TauIm][HSO<sub>4</sub>] is used. To do so, we selected PMI<sub>TOTAL</sub> as the green metric, which is divided into two terms: (i) PMI<sub>RRC</sub> for EL production (PMI<sub>EL</sub>) and (ii) PMI for the pretreatment step (PMI<sub>PT</sub>). For pretreatment, contributions from each component (chemicals, solvent, and workup) were considered. However, for the conversion step, since the bulk of the system refers to the green solvent ethanol (which could also be recycled), the PMI takes into account only the other chemicals for the EL synthesis. The PMI values are presented in Table 5.

**Table 5. PMI Values for EL Production from Raw and Pretreated SCBs**

SCB	PMI <sub>EL</sub>	PMI <sub>PT</sub>	PMI <sub>TOTAL</sub>
raw	26.9		26.9
PT—acid	40.2	60.6	100.8
PT—organosolv	27.1	90.6	117.7
PT—acid–base	24.8	278.2	303.0

According to Table 5, SCB obtained after the acid pretreatment presented the most divergent PMI value for EL production among the SCB feedstocks (PMI<sub>EL</sub> = 40.2). However, in terms of pretreatment, acidic conditions afforded the method with the greener credentials (PMI<sub>PT</sub> = 60.6), which corroborates with the EL and pretreatment yields presented in Table 3 (44% and 68%, respectively). The opposite tendency is observed for the sequential acid–base pretreatment, which showed the best value for PMI<sub>EL</sub> (24.8) and the higher PMI<sub>PT</sub> (278.2). This tendency also corroborates with Table 3 since high EL yields were achieved (55%), while the two-step process provided the lowest pretreatment yield (32%). According to this data, the complete evaluation of the process proved that using raw SCB is the greenest approach for EL production among the conditions evaluated in our study. This observation corroborates with the mass yields presented in Figure 4, demonstrating the higher production from raw SCB (38 g EL/100 g SCB) compared to pretreated materials (below 20 g EL/100 g SCB).

In addition to the quantitative evaluation using green metrics, our one-pot approach for EL production from raw feedstocks follows at least 7 of the 12 principles of Green Chemistry, namely, (1) prevent waste by using raw lignocellulose materials, which are considered residues from the agroindustry; (2) less hazardous synthesis by choosing the Debus–Radziszewski methodology for IL synthesis, using low toxicity reactants to form the imidazole ring; (3) design benign chemicals by producing EL, which is an essential biobased building block for industrial applications; (4) benign solvents and auxiliaries, once only green solvents were used in this work, including water, ethanol, and ILs; (5) design for energy efficiency using microwave irradiation for EL production; (6) the core of this work, the use of renewable feedstocks, by using agroindustrial residues as a feedstock for EL production, and using a renewable source of sulfonic acid, such as taurine, to synthesize protic IL;

and last but not least (7) catalysis, from the IL bifunctional role that acts as a solvent and catalyst providing the chemical conversion.

## CONCLUSIONS

EL was successfully produced from raw feedstocks mediated by a green taurine-derived IL, [TauIm][HSO<sub>4</sub>], under microwave irradiation. According to the experimental design for MCC conversion, the highest yield (above 80%) was achieved at the upper levels of the factors: 190 °C, 60 min, and 10 equiv of [TauIm][HSO<sub>4</sub>]. Moreover, the cellulose conversion to EL proved to be a complex system; indeed, the statistical model that described the microcrystalline cellulose conversion to EL was a reduced cubic model.

The computational analysis demonstrated that the cellobiose–IL complex has higher stabilization energy than the IL. In addition, the data confirmed the important role of the anion in cellulose deconstruction, in which it permeates between chains and disrupts the extensive network of hydrogen bonds between strands. The imidazolium cation then acts as a spacer, thus facilitating cellulose solubilization and, ultimately, its chemical conversion. Sugarcane bagasse proved to be the most promising biomass for EL production among the evaluated biomasses, affording EL up to 59% yield. Furthermore, no pretreatment was needed to achieve high EL yields, contributing to the feasibility of the process. Indeed, the evaluation of the process by using two green chemistry metrics (PMI and RP) corroborates the good overall greenness of the method based on the use of a novel taurine-derived IL, [TauIm][HSO<sub>4</sub>]. According to the results obtained with several lignocellulosic substrates, hemicelluloses play an essential role in EL production due to the more straightforward conversion in the acidic media than cellulose. In contrast, lignin did not significantly influence EL production, demonstrating the efficiency of the IL synthesized from taurine.

## ASSOCIATED CONTENT

### Supporting Information

The Supporting Information is available free of charge at <https://pubs.acs.org/doi/10.1021/acssuschemeng.2c05172>.

NMR spectra of the [TauIm] zwitterion and [TauIm][HSO<sub>4</sub>]; statistical analysis: ANOVA and predict vs observed graphic for EL production from MCC; computational analysis: complexes from the interactions and complexation energy calculations; feedstock chemical composition; and correlation between hemicelluloses and EL yields ([PDF](#))

## AUTHOR INFORMATION

### Corresponding Authors

Camila A. Rezende – Institute of Chemistry, University of Campinas - UNICAMP, 13083-970 Campinas, SP, Brazil;  
Email: [camilaiq@unicamp.br](mailto:camilaiq@unicamp.br)

Julio C. Pastre – Institute of Chemistry, University of Campinas - UNICAMP, 13083-970 Campinas, SP, Brazil;  
[ORCID: 0000-0001-9972-425X](https://orcid.org/0000-0001-9972-425X); Email: [jpastre@unicamp.br](mailto:jpastre@unicamp.br)

### Authors

Gustavo R. Gomes – Institute of Chemistry, University of Campinas - UNICAMP, 13083-970 Campinas, SP, Brazil  
Eupídio Scopel – Institute of Chemistry, University of Campinas - UNICAMP, 13083-970 Campinas, SP, Brazil

Nicola L. Rocha — Institute of Chemistry, University of Campinas - UNICAMP, 13083-970 Campinas, SP, Brazil  
Márcia C. Breitkreitz — Institute of Chemistry, University of Campinas - UNICAMP, 13083-970 Campinas, SP, Brazil  
Rodrigo A. Cormanich — Institute of Chemistry, University of Campinas - UNICAMP, 13083-970 Campinas, SP, Brazil;  
ORCID: orcid.org/0000-0001-7659-1749

Complete contact information is available at:  
<https://pubs.acs.org/10.1021/acssuschemeng.2c05172>

## Author Contributions

<sup>‡</sup>G.R.G. and E.S. contributed equally to this work.

## Notes

The authors declare no competing financial interest.

## ACKNOWLEDGMENTS

The authors gratefully acknowledge financial support from the São Paulo Research Foundation—FAPESP (Award N.: J.C.P., 2014/26378-2, 2014/25770-6, 2020/11578-7, and 2021/06661-5; G.R.G., 2018/09861-2; C.A.R., 2018/23769-1; E.S., 2019/19360-3; R.A.C., 2018/03910-1), the Brazilian National Council for Scientific and Technological Development—CNPq (C.A.R., 420031/2018-9; G.R.G., 142278/2017-3; E.S., 142570/2019-2), and the Coordination for the Improvement of Higher Education Personnel (CAPES, NLR, Finance Code 001). CENAPAD-SP, CESUP, and SDumont computational resources are also gratefully acknowledged.

## REFERENCES

- (1) Maity, S. K. Opportunities, Recent Trends, and Challenges of Integrated Biorefinery: Part I. *Renewable Sustainable Energy Rev.* **2015**, *43*, 1427–1445.
- (2) Yan, L.; Yao, Q.; Fu, Y. Conversion of Levulinic Acid and Alkyl Levulinate into Biofuels and High-Value Chemicals. *Green Chem.* **2017**, *19*, 5527–5547.
- (3) Kuwahara, Y.; Kaburagi, W.; Nemoto, K.; Fujitani, T. Esterification of Levulinic Acid with Ethanol over Sulfated Si-Doped ZrO<sub>2</sub> Solid Acid Catalyst: Study of the Structure-Activity Relationships. *Appl. Catal., A* **2014**, *476*, 186–196.
- (4) Li, N.; Jiang, S.; Liu, Z. Y.; Guan, X. X.; Zheng, X. C. Preparation and Catalytic Performance of Loofah Sponge-Derived Carbon Sulfonic Acid for the Conversion of Levulinic Acid to Ethyl Levulinate. *Catal. Commun.* **2019**, *121*, 11–14.
- (5) Tiong, Y. W.; Yap, C. L.; Gan, S.; Yap, W. S. P. One-Pot Conversion of Oil Palm Empty Fruit Bunch and Mesocarp Fiber Biomass to Levulinic Acid and Upgrading to Ethyl Levulinate via Indium Trichloride-Ionic Liquids. *J. Cleaner Prod.* **2017**, *168*, 1251–1261.
- (6) Pace, V.; Hoyos, P.; Castoldi, L.; Domínguez De María, P.; Alcántara, A. R. 2-Methyltetrahydrofuran (2-MeTHF): A Biomass-Derived Solvent with Broad Application in Organic Chemistry. *ChemSusChem* **2012**, *5*, 1369–1379.
- (7) Kuwahara, Y.; Kango, H.; Yamashita, H. Catalytic Transfer Hydrogenation of Biomass-Derived Levulinic Acid and Its Esters to  $\gamma$ -Valerolactone over Sulfonic Acid-Functionalized UiO-66. *ACS Sustainable Chem. Eng.* **2017**, *5*, 1141–1152.
- (8) Ye, F.; Zhang, D.; Xue, T.; Wang, Y.; Guan, Y. Enhanced Hydrogenation of Ethyl Levulinate by Pd–AC Doped with Nb<sub>2</sub>O<sub>5</sub>. *Green Chem.* **2014**, *16*, 3951–3957.
- (9) Xue, Z.; Yu, D.; Zhao, X.; Mu, T. Upgrading of Levulinic Acid into Diverse N-Containing Functional Chemicals. *Green Chem.* **2019**, *21*, 5449–5468.
- (10) Wu, J.; Gao, G.; Sun, P.; Long, X.; Li, F. Synergetic Catalysis of Bimetallic CuCo Nanocomposites for Selective Hydrogenation of Bioderived Esters. *ACS Catal.* **2017**, *7*, 7890–7901.
- (11) Zhuang, X.; Wang, W.; Yu, Q.; Qi, W.; Wang, Q.; Tan, X.; Zhou, G.; Yuan, Z. Liquid Hot Water Pretreatment of Lignocellulosic Biomass for Bioethanol Production Accompanying with High Valuable Products. *Bioresour. Technol.* **2016**, *199*, 68–75.
- (12) Chio, C.; Sain, M.; Qin, W. Lignin Utilization: A Review of Lignin Depolymerization from Various Aspects. *Renewable Sustainable Energy Rev.* **2019**, *107*, 232–249.
- (13) Kang, S.; Fu, J.; Zhang, G. From Lignocellulosic Biomass to Levulinic Acid: A Review on Acid-Catalyzed Hydrolysis. *Renewable Sustainable Energy Rev.* **2018**, *94*, 340–362.
- (14) Hayes, R.; Warr, G. G.; Atkin, R. Structure and Nanostructure in Ionic Liquids. *Chem. Rev.* **2015**, *115*, 6357–6426.
- (15) Hulsbosch, J.; De Vos, D. E.; Binnemans, K.; Ameloot, R. Biobased Ionic Liquids: Solvents for a Green Processing Industry? *ACS Sustainable Chem. Eng.* **2016**, *4*, 2917–2931.
- (16) van Rantwijk, F.; Sheldon, R. A. Biocatalysis in Ionic Liquids. *Chem. Rev.* **2007**, *107*, 2757–2785.
- (17) Usmani, Z.; Sharma, M.; Gupta, P.; Karpichev, Y.; Gathergood, N.; Bhat, R.; Gupta, V. K. Ionic Liquid Based Pretreatment of Lignocellulosic Biomass for Enhanced Bioconversion. *Bioresour. Technol.* **2020**, *304*, No. 123003.
- (18) Zhang, J.; Zou, D.; Singh, S.; Cheng, G. Recent Developments in Ionic Liquid Pretreatment of Lignocellulosic Biomass for Enhanced Bioconversion. *Sustainable Energy Fuels* **2021**, *5*, 1655–1667.
- (19) Dotsenko, A. S.; Dotsenko, G. S.; Senko, O. V.; Stepanov, N. A.; Lyagin, I. V.; Efremenko, E. N.; Gusakov, A. V.; Zorov, I. N.; Rubtsova, E. A. Complex Effect of Lignocellulosic Biomass Pretreatment with 1-Butyl-3-Methylimidazolium Chloride Ionic Liquid on Various Aspects of Ethanol and Fumaric Acid Production by Immobilized Cells within SSF. *Bioresour. Technol.* **2018**, *250*, 429–438.
- (20) Ramos, L. P.; da Silva, L.; Ballem, A. C.; Pitarelo, A. P.; Chiarello, L. M.; Silveira, M. H. L. Enzymatic Hydrolysis of Steam-Exploded Sugarcane Bagasse Using High Total Solids and Low Enzyme Loadings. *Bioresour. Technol.* **2015**, *175*, 195–202.
- (21) Yuan, X.; Duan, Y.; He, L.; Singh, S.; Simmons, B.; Cheng, G. Characterization of White Poplar and Eucalyptus after Ionic Liquid Pretreatment as a Function of Biomass Loading Using X-Ray Diffraction and Small Angle Neutron Scattering. *Bioresour. Technol.* **2017**, *232*, 113–118.
- (22) Uto, T.; Yamamoto, K.; Kadokawa, J. I. Cellulose Crystal Dissolution in Imidazolium-Based Ionic Liquids: A Theoretical Study. *J. Phys. Chem. B* **2018**, *122*, 258–266.
- (23) Dissanayake, N.; Thalangamaarachchige, V. D.; Troxell, S.; Quitevis, E. L.; Abidi, N. Substituent Effects on Cellulose Dissolution in Imidazolium-Based Ionic Liquids. *Cellulose* **2018**, *25*, 6887–6900.
- (24) Paiva, T. G.; Zanatta, M.; Cabrita, E. J.; Bernardes, C. E. S.; Corvo, M. C. DMSO/IL Solvent Systems for Cellulose Dissolution: Binary or Ternary Mixtures? *J. Mol. Liq.* **2022**, *345*, No. 117810.
- (25) Silveira, M. H. L.; Morais, A. R. C.; da Costa Lopes, A. M.; Olekszyszn, D. N.; Bogel-Lukasik, R.; Andreaus, J.; Ramos, L. P. Current Pretreatment Technologies for the Development of Cellulosic Ethanol and Biorefineries. *ChemSusChem* **2015**, *8*, 3366–3390.
- (26) Zhang, Y.; Wang, X.; Hou, T.; Liu, H.; Han, L.; Xiao, W. Efficient Microwave-Assisted Production of Biofuel Ethyl Levulinate from Corn Stover in Ethanol Medium. *J. Energy Chem.* **2018**, *27*, 890–897.
- (27) Chang, C.; Xu, G.; Jiang, X. Production of Ethyl Levulinate by Direct Conversion of Wheat Straw in Ethanol Media. *Bioresour. Technol.* **2012**, *121*, 93–99.
- (28) Ramli, N. A. S.; Amin, N. A. S. Catalytic Conversion of Carbohydrate Biomass in Ionic Liquids to 5-Hydroxymethyl Furfural and Levulinic Acid: A Review. *Bioenergy Res.* **2020**, *13*, 693–736.
- (29) da Costa Lopes, A. M.; Bogel-Lukasik, R. Acidic Ionic Liquids as Sustainable Approach of Cellulose and Lignocellulosic Biomass Conversion without Additional Catalysts. *ChemSusChem* **2015**, *8*, 947–965.
- (30) Gong, C.; Wei, J.; Tang, X.; Zeng, X.; Sun, Y.; Lin, L. Production of Levulinic Acid and Ethyl Levulinate from Cellulosic Pulp Derived from the Cooking of Lignocellulosic Biomass with Active Oxygen and Solid Alkali. *Korean J. Chem. Eng.* **2019**, *36*, 740–752.

- (31) Liu, H.; Zhang, Y. X.; Hou, T.; Chen, X.; Gao, C.; Han, L.; Xiao, W. Mechanical Deconstruction of Corn Stover as an Entry Process to Facilitate the Microwave-Assisted Production of Ethyl Levulinate. *Fuel Process. Technol.* **2018**, *174*, 53–60.
- (32) Guan, Q.; Lei, T.; Wang, Z.; Xu, H.; Lin, L.; Chen, G.; Li, X.; Li, Z. Preparation of Ethyl Levulinate from Wheat Straw Catalysed by Sulfonate Ionic Liquid. *Ind. Crops Prod.* **2018**, *113*, 150–156.
- (33) Tiong, Y. W.; Yap, C. L.; Gan, S.; Yap, W. S. P. Optimisation Studies on the Conversion of Oil Palm Biomass to Levulinic Acid and Ethyl Levulinate via Indium Trichloride-Ionic Liquids: A Response Surface Methodology Approach. *Ind. Crops Prod.* **2019**, *128*, 221–234.
- (34) Anastas, P. T. *Green Solvents Volume 6: Ionic Liquids*, 2010.
- (35) Esposito, D.; Kirchhecker, S.; Antonietti, M. A Sustainable Route towards Imidazolium Building Blocks Based on Biomass Molecules. *Chem. - Eur. J.* **2013**, *19*, 15097–15100.
- (36) Kirchhecker, S.; Antonietti, M.; Esposito, D. Hydrothermal Decarboxylation of Amino Acid Derived Imidazolium Zwitterions: A Sustainable Approach towards Ionic Liquids. *Green Chem.* **2014**, *16*, 3705–3709.
- (37) Sarkar, P.; Basak, P.; Ghosh, S.; Kundu, M.; Sil, P. C. Prophylactic Role of Taurine and Its Derivatives against Diabetes Mellitus and Its Related Complications. *Food Chem. Toxicol.* **2017**, *110*, 109–121.
- (38) Shirini, F.; Daneshvar, N. Introduction of Taurine (2-Aminoethanesulfonic Acid) as a Green Bio-Organic Catalyst for the Promotion of Organic Reactions under Green Conditions. *RSC Adv.* **2016**, *6*, 110190–110205.
- (39) Kvasnička, F.; Rajchl, A. Electrophoretic Determination of Taurine. *J. Chromatogr. A* **2021**, *1645*, No. 462075.
- (40) Rodrigues Gomes, G.; Breitkreitz, M. C.; Pastre, J. C. Ash Influence on the Ethyl Levulinate Production from Sugarcane Molasses Mediated by Taurine Hydrogen Sulfate. *ACS Sustainable Chem. Eng.* **2021**, *9*, 13438–13449.
- (41) Albert-Soriano, M.; Hernández-Martínez, L.; Pastor, I. M. 1,3-Bis(Carboxymethyl)Imidazolium Chloride as a Metal-Free and Recyclable Catalyst for the Synthesis of N-Allylanilines by Allylic Substitution of Alcohols. *ACS Sustainable Chem. Eng.* **2018**, *6*, 14063–14070.
- (42) Bowers, K. J.; Chow, E.; Xu, H.; Dror, R. O.; Eastwood, M. P.; Gregersen, B. A.; Klepeis, J. L.; Kolossvary, I.; Moraes, M. A.; Sacerdoti, F. D.; Salmon, J. K.; Shan, Y.; Shaw, D. E. In *Scalable Algorithms for Molecular Dynamics Simulations on Commodity Clusters*, Proceedings of the 2006 ACM/IEEE Conference on Supercomputing: SC'06, Vol 84, 2006.
- (43) Zhao, Y.; Truhlar, D. G. The M06 Suite of Density Functionals for Main Group Thermochemistry, Thermochemical Kinetics, Non-covalent Interactions, Excited States, and Transition Elements: Two New Functionals and Systematic Testing of Four M06-Class Functionals and 12 Other Function. *Theor. Chem. Acc.* **2008**, *120*, 215–241.
- (44) Burns, L. A.; Vázquez-Mayagoitia, Á.; Sumpter, B. G.; Sherrill, C. D. Density-Functional Approaches to Noncovalent Interactions: A Comparison of Dispersion Corrections (DFT-D), Exchange-Hole Dipole Moment (XDM) Theory, and Specialized Functionals. *J. Chem. Phys.* **2011**, *134*, No. 084107.
- (45) Frisch, M. J.; Trucks, G. W.; Schlegel, H. B.; Scuseria, G. E.; Robb, M. A.; Cheeseman, J. R.; Scalmani, G.; Barone, V.; Petersson, G. A.; Nakatsuji, H.; Li, X.; Caricato, M.; Marenich, A.; Bloino, J.; Janesko, B. G.; Gomperts, R.; Mennucci, B. Gaussian 09, Revision A.02, Wallingford CT, 2016.
- (46) Scalmani, G.; Frisch, M. J. Continuous Surface Charge Polarizable Continuum Models of Solvation. I. General Formalism. *J. Chem. Phys.* **2010**, *132*, No. 114110.
- (47) Simon, S.; Duran, M.; Dannenberg, J. J. How Does Basis Set Superposition Error Change the Potential Surfaces for Hydrogen-bonded Dimers? *J. Chem. Phys.* **1996**, *105*, 11024–11031.
- (48) Neese, F. Software Update: The ORCA Program System, Version 4.0. *Wiley Interdiscip. Rev. Comput. Mol. Sci.* **2018**, *8*, No. e1327.
- (49) Altun, A.; Neese, F.; Bistoni, G. HFID: A Nonempirical London Dispersion-Corrected Hartree–Fock Method for the Quantification and Analysis of Noncovalent Interaction Energies of Large Molecular Systems. *J. Chem. Theory Comput.* **2019**, *15*, 5894–5907.
- (50) Bader, R. F. W. *Atoms in Molecules: A Quantum Theory*; Clarendon: Oxford, 1990.
- (51) Sluiter, A.; Hames, B.; Ruiz, R.; Scarlata, C.; Sluiter, J.; Templeton, D.; NREL, D. C. Determination of Structural Carbohydrates and Lignin in Biomass NREL/TP-510-42618. *NREL – Natl. Renew. Energy Lab.* 2012.
- (52) Sluiter, A.; Ruiz, R.; Scarlata, C.; Sluiter, J.; Templeton, D. *Determination of Extractives in Biomass Laboratory Analytical Procedure (LAP)*. Issue Date: 7/17/2005 *Determination of Extractives in Biomass Laboratory Analytical Procedure (LAP)*. 2008, No. January.
- (53) Sluiter, A.; Hames, B.; Ruiz, R.; Scarlata, C.; Sluiter, J.; Templeton, D. *Determination of Ash in Biomass NREL/TP-510-42622*. *NREL – Natl. Renew. Energy Lab.* 2008.
- (54) Scopel, E.; Rezende, C. A. Biorefinery On-Demand: Modulating Pretreatments to Recover Lignin, Hemicellulose, and Extractives as Co-Products during Ethanol Production. *Ind. Crops Prod.* **2021**, *163*, No. 113336.
- (55) Gomes, G. R.; Rampon, D. S.; Ramos, L. P. Production of 5-(Hydroxymethyl)-Furfural from Water-Soluble Carbohydrates and Sugarcane Molasses. *Appl. Catal., A* **2017**, *545*, 127–133.
- (56) Gomes, G. R.; Rampon, D. S.; Ramos, L. P. Production of Furan Compounds from Sugarcane Bagasse Using a Catalytic System Containing ZnCl<sub>2</sub>/HCl or AlCl<sub>3</sub>/HCl in a Biphasic System. *J. Braz. Chem. Soc.* **2018**, *29*, 1115–1122.
- (57) Gomes, G. R.; Pastre, J. C. Microwave-Assisted HMF Production from Water-Soluble Sugars Using Betaine-Based Natural Deep Eutectic Solvents (NADES). *Sustainable Energy Fuels* **2020**, *4*, 1891–1898.
- (58) Ramos, L. P. The Chemistry Involved in the Steam Treatment of Lignocellulosic Materials. *Quim. Nova* **2003**, *26*, 863–871.
- (59) Chemcraft - graphical software for visualization of quantum chemistry computations.
- (60) Keith, T. A.; AIMAll, T. K. Gristmill Software: Overland Park KS, USA, 2019.
- (61) Companhia Nacional de Abastecimento - (CONAB). Acompanhamento da Safra Brasileira - CANA-DE-AÇÚCAR SAFRA 2021/22- 2ºLEVANTAMENTO. In *Acompanhamento da Safra Brasileira - CANA-DE-AÇÚCAR SAFRA 2021/22-2ºLEVANTAMENTO*; 2021; pp 1–63.
- (62) Zhu, H.; Luo, W.; Ciesielski, P. N.; Fang, Z.; Zhu, J. Y.; Henriksson, G.; Himmel, M. E.; Hu, L. Wood-Derived Materials for Green Electronics, Biological Devices, and Energy Applications. *Chem. Rev.* **2016**, *116*, 9305–9374.
- (63) Ahmad, E.; Alam, I.; Pant, K. K.; Haider, M. A. Catalytic and Mechanistic Insights into the Production of Ethyl Levulinate from Biorenewable Feedstocks. *Green Chem.* **2016**, *18*, 4804–4823.
- (64) Marçon, H. M.; Pastre, J. C. Continuous Flow Meerwein-Ponndorf-Verley Reduction of HMF and Furfural Using Basic Zirconium Carbonate. *RSC Adv.* **2022**, *12*, 7980–7989.
- (65) Liu, Y.; Liu, X.; Li, M.; Meng, Y.; Li, J.; Zhang, Z.; Zhang, H. Recyclable Zr/Hf-Containing Acid-Base Bifunctional Catalysts for Hydrogen Transfer Upgrading of Biofurans: A Review. *Front. Chem.* **2021**, *9*, No. 812331.
- (66) Negrão, D. R.; Grandis, A.; Buckeridge, M. S.; Rocha, G. J. M.; Leal, M. R. L. V.; Driemeier, C. Inorganics in Sugarcane Bagasse and Straw and Their Impacts for Bioenergy and Biorefining: A Review. *Renewable Sustainable Energy Rev.* **2021**, *148*, No. 111268.
- (67) Monteith, E. R.; Mampuys, P.; Summerton, L.; Clark, J. H.; Maes, B. U. W.; McElroy, C. R. Why We Might Be Misusing Process Mass Intensity (PMI) and a Methodology to Apply It Effectively as a Discovery Level Metric. *Green Chem.* **2020**, *22*, 123–135.
- (68) McElroy, C. R.; Constantinou, A.; Jones, L. C.; Summerton, L.; Clark, J. H. Towards a Holistic Approach to Metrics for the 21st Century Pharmaceutical Industry. *Green Chem.* **2015**, *17*, 3111–3121.
- (69) Liao, Q.; Liu, W.; Meng, Z. Strategies for Overcoming the Limitations of Enzymatic Carbon Dioxide Reduction. *Biotechnol. Adv.* **2022**, *60*, No. 108024.

- (70) Koschmieder, J.; Alseekh, S.; Shabani, M.; Baltenweck, R.; Maurino, V. G.; Palme, K.; Fernie, A. R.; Hugueney, P.; Welsch, R. Color Recycling: Metabolization of Apocarotenoid Degradation Products Suggests Carbon Regeneration via Primary Metabolic Pathways. *Plant Cell Rep.* **2022**, *41*, 961–977.
- (71) Chen, J.; Zhao, G.; Chen, L. Efficient Production of 5-Hydroxymethylfurfural and Alkyl Levulinate from Biomass Carbohydrate Using Ionic Liquid-Based Polyoxometalate Salts. *RSC Adv.* **2014**, *4*, 4194–4202.
- (72) Naz, S.; Uroos, M.; Muhammad, N. Effect of Molecular Structure of Cation and Anions of Ionic Liquids and Co-Solvents on Selectivity of 5-Hydroxymethylfurfural from Sugars, Cellulose and Real Biomass. *J. Mol. Liq.* **2021**, *334*, No. 116523.
- (73) Lee, V. Y.; McNiece, K.; Ito, Y.; Sekiguchi, A.; Geinik, N.; Becker, J. Y. Tetrakis(Di-Tert-Butylmethylsilyl)Digermene: Synthesis, Structure, Electrochemical Properties, and Reactivity. *Heteroat. Chem.* **2014**, *25*, 313–319.
- (74) Li, H.; Yang, S. Catalytic Transformation of Fructose and Sucrose to HMF with Proline-Derived Ionic Liquids under Mild Conditions. *Int. J. Chem. Eng.* **2014**, *2014*, No. 978708.

### ■ NOTE ADDED AFTER ASAP PUBLICATION

Due to a production error, this article originally published with an incorrect Supporting Information file. The correct file published December 5, 2022.

## □ Recommended by ACS

### Efficient Biomass Pretreatment Process Based on the Simple Reuse of a Low-Viscosity Ionic-Liquid Solvent System

Jiming Yang, Suojiang Zhang, *et al.*

SEPTEMBER 13, 2022

ACS SUSTAINABLE CHEMISTRY & ENGINEERING

READ

### Insight into the Mechanism of Humic Acid's Dissolution Capacity for Lignin in the Biomass Substrates

Wei Tang, Qiang Yong, *et al.*

OCTOBER 26, 2022

ACS SUSTAINABLE CHEMISTRY & ENGINEERING

READ

### Competition of Dual Roles of Ionic Liquids during In Situ Transesterification of Wet Algae

Dan Ding, Yingqiang Sun, *et al.*

SEPTEMBER 30, 2022

ACS SUSTAINABLE CHEMISTRY & ENGINEERING

READ

### Hydrotreatment of Supercritical Carbon Dioxide Extracts of Hydrothermal Liquefaction Lignocellulosic Biocrude

Nikolaos Montesantos, Marco Maschietti, *et al.*

OCTOBER 06, 2022

INDUSTRIAL & ENGINEERING CHEMISTRY RESEARCH

READ

Get More Suggestions >